Journal of Materials Chemistry C

RSC Publishing

PAPER

View Article Online
View Journal | View Issue

Cite this: J. Mater. Chem. C, 2013, 1, 7842

Soft biomimetic tapered nanostructures for large-area antireflective surfaces and SERS sensing†

Bihter Daglar,[ab] Tural Khudiyev,[ab] Gokcen Birlik Demirel,[ad] Fatih Buyukserin[e] and Mehmet Bayindir*[abc]

Received 16th August 2013
Accepted 20th September 2013

DOI: 10.1039/c3tc31616e

www.rsc.org/MaterialsC

We report a facile fabrication method for the fabrication of functional large area nanostructured polymer films using a drop casting technique. Reusable and tapered silicon molds were utilized in the production of functional polymers providing rapid fabrication of the paraboloid nanostructures at the desired structural heights without the requirement of any complex production conditions, such as high temperature or pressure. The fabricated polymer films demonstrate promising qualities in terms of antireflective, hydrophobic and surface enhanced Raman spectroscopy (SERS) features. We achieved up to 92% transmission from the single-side nanostructured polymer films by implementing optimized nanostructure parameters which were determined using a finite difference time domain (FDTD) method prior to production. Large-area nanostructured films were observed to enhance the Raman signal with an enhancement factor of 4.9×10^6 compared to bare film, making them potentially suitable as free-standing SERS substrates. The utilized fabrication method with its demonstrated performances and reliable material properties, paves the way for further possibilities in biological, optical, and electronic applications.

Introduction

Nature inspires scientists with the ordered nipple-like structures in the eyes of insects (such as moths and butterflies) or with the multi-functional surfaces of gecko feet and lotus leaves.[1–4] A number of lithography techniques have been developed to fabricate these bio-inspired architectures: paraboloid, triangular, cylindrical, or conical structures, for their use in optical and electronic applications.[5–7] Thanks to advances in fabrication and characterization techniques, various properties can be successfully transferred from nature, such as excellent adhesion, antireflectivity, and self-cleaning. Hence, utilizing these micro–nano structures may bring many conveniences into our daily life.

One of the possible applications of biomimetics is antireflective surfaces. Reflection occurs due to the refractive index difference of the two media, and is explained with Fresnel equations which state that a bigger refractive index difference would lead to more reflection. Tapered structures with paraboloid, conic or triangular shapes provide superior anti-reflective properties due to the gradual change of refractive index between these structures and the surrounding air.[8–11] Alternatively, anti-reflection coatings (single/multi-layer films) are used in order to prevent reflection.[12–15] However, they are inefficient in terms of angle-dependence and are feasible only for narrowband applications. Therefore, anti-reflective structures (ARSs) are essential for optical devices, solar cells, light emitting diodes (LEDs), and displays in order to prevent undesired reflection.[16,17]

Biomimetic surfaces are also used as efficient SERS substrates for the detection of small amounts of molecules, even down to the single-molecule level.[18] Raman signals can be enhanced electromagnetically and chemically using particular SERS substrates. Hot spots created by plasmonic nanostructures (*i.e.* electromagnetic enhancement) are responsible for the major portion of SERS enhancement. However, it is still a big challenge to produce large-area and reproducible SERS substrates and designed biomimetic surfaces may fill this demand.

There are many production techniques to fabricate biomimetic micro–nano structures, including nano-sphere lithography, laser-interference lithography, decal transfer lithography,

[a]UNAM-National Nanotechnology Research Center, Bilkent University, 06800 Ankara, Turkey. E-mail: bayindir@nano.org.tr

[b]Institute of Materials Science and Nanotechnology, Bilkent University, 06800 Ankara, Turkey

[c]Department of Physics, Bilkent University, 06800 Ankara, Turkey

[d]Department of Chemistry, Gazi University, Polatli, 06900 Ankara, Turkey

[e]Department of Biomedical Engineering, TOBB University, 06560 Ankara, Turkey

† Electronic supplementary information (ESI) available: Experimental and calculation details for the SERS substrates, detailed etch conditions of the silicon molds, SEM images of PC paraboloids after using the silicon mold ten times, transmission measurements of PC paraboloids for a wavelength range of 800–2200 nm, comparison of simulated and measured transmission spectrum of nanostructured films, and CA measurements of PC films and silicon molds. See DOI: 10.1039/c3tc31616e

nanoimprinting lithography, and plasma etching, which are used on various substrates such as glass, silicon, polymers, *etc.*[19–26] Nanostructured polymeric materials in particular, are attracting interest due to their wide usage in biomolecular sensing, optics and optoelectronic applications.[27–30] In order to produce polymer nanostructures, hot embossing through a mold is applied in the pre-mentioned fabrication techniques. During the hot embossing procedure, the system is heated above the glass transition temperature of the polymer and a desired pressure is applied.[31–34] The utilized molds are composed of different types of materials, such as anodized aluminum oxide, silicon, or polymers.[35–39]

Bowen *et al.* described a new soft-lithography patterning technique to fabricate elastomeric stamps by decal transfer lithography with triangular cross sections.[40] Fabricated micron-scale poly(dimethylsiloxane) (PDMS) decals indicate well-controlled light–matter interactions and show antireflective properties. The produced surface is used as a SERS substrate efficiently, however multi-step production and an embossing step is required. In an alternative route, Choi *et al.* proposed the fabrication of a tapered shape mold to produce paraboloid nanostructures composed of poly(methyl methacrylate) (PMMA).[41] In this method, an anodized aluminum oxide (AAO) membrane is used as a mold and the tapered shape is acquired by multistep anodization and chemical etching processes. Reflection of the PMMA surface is dramatically reduced, but the multistep produced AAO mold is not reusable and repeated fabrication is required for each AAO mold. Eventually, the fabrication of the nanostructured polymers requires multiple production steps or specific conditions.

In this study, we proposed a facile method for the large-area production of biomimetic nanostructures that utilize reusable silicon molds and drop casting at ambient conditions to overcome complex environment requirements and multistep fabrication processes. To produce silicon molds, AAO membranes are used as a mask during plasma etching and tapered nanopores are formed at the desired lengths with high packing density. Polymer nanostructures are fabricated by drop casting of the polymer solution directly on the silicon molds. In order to obtain the maximum antireflection performance, design parameters of the 3D nanostructures were simulated using an FDTD method prior to the fabrication process. Inductively coupled plasma (ICP) etch conditions (*i.e.* process duration and pressure) were optimized for obtaining the desired lengths and structure profile. Polycarbonate (PC) was chosen due to its high-transmittance, biocompatibility, durability, high impact resistance, and wide usage in electronic components.[42,43] On the other hand, the utilized PC material possesses a moderate refractive index and ignorable absorption in the visible wavelengths, which makes it feasible for optical applications. Besides the antireflection feature, produced tapered structures exhibit highly hydrophobic properties (145° water contact angle). We also demonstrated our nanostructured polymer surfaces as a free-standing SERS substrate and observed a 4.9×10^6 enhancement factor in *average SERS* experiments. A prominent feature of our facile fabrication method is its versatile nature that it can allow the production of biomimetic nanostructures from different kinds of polymers and other moldable materials.

Experimental section

FDTD simulations

FDTD simulations were performed using a commercial finite-difference time-domain software (Lumerical Solutions Inc.). Simulations were done in three dimensional simulation regions. We illuminated our structure with a broadband (400–800 nm) planewave source. Frequency-domain power monitors were used to collect the reflected and transmitted light using 500 wavelength points. To decrease the simulation time we used periodic boundary conditions. To obtain a transmission *versus* height plot for double side and single side structure cases we averaged the spectrum (400–800 nm wavelengths) in each height point. Shapes of the structures were derived with related equations which define their edges. Edges of the paraboloid (convex), paraboloid (concave), and cone shapes are proportional with the equations $y = ax^2$, $y = bx^{1/2}$, and $y = cx$, respectively.

Fabrication of the silicon mold

The free-standing AAO membranes were obtained by a voltage reduction protocol[44] and were used as etch masks to fabricate the silicon molds.[37] First, nanoporous AAO films were formed on both sides of the Al foil by a two-step anodization method. Here, high purity Al foil (99.998%) was polished with sand paper and then electropolished at 15 V in a solution containing 95 wt% H_3PO_4, 5 wt% H_2SO_4 and 20 g l^{-1} of CrO_3. The Al foil was then anodized in 5 wt% aqueous oxalic acid solution at 8 °C under 50 V against a stainless-steel cathode. After a 16 h long first anodization, the alumina film was dissolved in acidic CrO_3 solution and a 10 min second anodization was carried out again under 50 V. At the end of this period, the voltage was gradually decreased to 15 V by making 5% voltage reductions every 2 min. In order to obtain free-standing AAO membranes, this sample was immersed in 10 wt% H_3PO_4 solution until rapid bubble formation was observed. The membranes were then collected from the Al surface using a thin parafilm backing paper.

p-Type silicon[100] wafer was cleaned before the ICP etching process (STS LPX SR F) with acetone, isopropanol, and water respectively. The AAO membrane was placed on the silicon surface with the branched layer side facing up using isopropanol. The branched layer of the AAO was removed by an Ar plasma pre-etching step (10 mTorr, 40 min). Tapered nanopores were formed using optimized mixtures of Ar and Cl_2 gases. Ar/Cl_2 plasma etch was applied in three steps in series for different pressures; 25 mTorr, 20 mTorr, and 5 mTorr, respectively. The plasma etching steps were accomplished in a few seconds and the detailed durations for the different nanostructure heights are given in the ESI, Table S1.† The AAO membrane was removed using 17% phosphoric acid and then the silicon surface was cleaned with 40% HF in 2 minutes. The silicon mold was coated with 1% (v/v) 1*H*,1*H*,2*H*,2*H*-perfluorodecyl-

trichloro silane (FDTS) in *n*-heptane. Coated silicon was cured at 100 °C under vacuum for 1 h.

Fabrication of the PC paraboloid nanostructures

PC solution (6%, w/v) in dichloromethane (DCM) solvent, was carefully drop casted on the silicon mold. An overnight waiting period allowed complete solvent evaporation and polymer diffusion into the pores at ambient conditions. The dried polymer was then peeled easily from the surface by hand. Bare films were produced using the same drop casting conditions as in the nanostructured films to prevent potential experimental errors in the optical measurements.

Surface characterization

Tapered nanostructures of the porous silicon mold were analyzed by a focused ion beam (FIB) (Nova 600i Nanolab) system and scanning electron microscopy (SEM) (Quanta 200 FEG). Using FIB, a cross section of the pore was cut by depositing platinum and then imaged by SEM. Fabricated PC paraboloid nanostructures were coated with Au/Pd using a precision etching coating system (PECS, Gatan 682) prior to SEM characterization to prevent charging, and then imaged with a tilting angle of 30°. The hydrophobicity of the PC films was characterized using a contact angle measurement system (Dataphysics, OCA 30). In addition, the fluorination of the silicon molds was controlled by checking their water contact angles (Fig. S4c and d†).

Optical measurements

The transmission and reflection of the bare and nanostructured films were determined by a spectrophotometer (Cary 5000 UV-Vis-NIR Spectrophotometer). Specular reflection was measured using an external DRA attachment for a wavelength range of 400 nm to 800 nm with a 1 nm interval.

SERS measurements

SERS and Raman spectra of the fabricated films were collected by a Raman module (WITEC Alpha 300S). Prior to the measurements, 150 nm nanostructured PC film and reference PC bare film were coated with 40 nm silver using a thermal evaporator. 5 μl of 10^{-7} M and 2 mM rhodamine 6G (R6G) solutions in ethanol were dropped on the nanostructured and bare film, respectively. SERS and Raman spectra were acquired by a 532 nm laser source at 50 μW power with 2 μm spot size.

Results and discussion

Fabrication of the silicon mold and biomimetic nanostructures

Biomimetic sub-wavelength paraboloid nanostructures on the polymer surfaces were produced *via* drop casting of the polymer solutions onto precise silicon molds which were produced according to the schematic given in Fig. 1a–c. AAO membranes with 50–60 nm pore sizes were used as ICP etch masks. AAO membranes offer a high-density ordered nanoporous

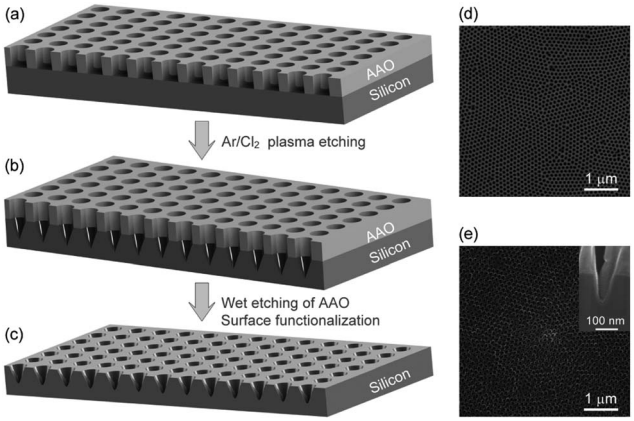

Fig. 1 Schematic representation of the silicon mold fabrication. (a) AAO membrane–silicon wafer [100] assembly is shown after the branched side of membrane is removed. (b) Tapered pores are formed in the silicon using an Ar/Cl_2 plasma etch in three steps. (c) The AAO membrane is removed from the silicon surface using phosphoric acid wet etching and then the mold pore is functionalized with fluorinated ligands. Cross section views of the etched silicon mold are also shown. Top view SEM images of (d) the AAO membrane and (e) the silicon mold after removing AAO membrane are given (the inset shows a cross section of the silicon pores, the sample was prepared using FIB). The SEM images show that the hexagonally packed uniform pores of the AAO membranes were successfully transferred to the silicon surface. In addition, the pore shape was obtained as paraboloid, which entails the best antireflective property for the PC nanostructures.

architecture with hexagonal symmetry. In the first step, the mask was placed on silicon wafer [100] and the branched side of the membrane was pre-etched by Ar plasma (Fig. 1d). Tapered structures of the nanopores were formed using Ar/Cl_2 plasma in ICP system in three steps in series for decreasing pressures. The detailed pressure and duration parameters of the plasma steps are given in Table S1.† After the plasma etching process, the AAO membrane was removed using a phosphoric acid wet etch and the silicon surface was cleaned with hydrofluoric acid (HF). Finally, the mold was coated with 1% (v/v) 1*H*,1*H*,2*H*,2*H*-perfluorodecyl-trichloro silane (FDTS) in *n*-heptane solution in order to prevent polymer adherence into the pores.

A top view SEM image of the silicon mold after removing the AAO mask is given in Fig. 1e. The formation of the tapered structures within the nanopores was proven by using the FIB technique and a cross section image of the pore was also introduced at the inset of Fig. 1e. As observed in the SEM images, silicon pores have a paraboloid shape and the aperture of the pores begins at 50–60 nm, which is consistent with the mask pores.

At the last step of our production method, drop casting was used at ambient conditions. On the contrary to other production techniques, drop casting doesn't require any complicated devices, or equipment. The PC solution (6%, w/v) was simply drop casted on the silicon mold, we waited for the solvent to evaporate, and then the formed film was peeled from the surface (Fig. 2a–c, ESI video†). Nanostructures at different heights were fabricated using appropriate molds. The area of the nanostructured surface directly depends on the large-area AAO membrane which was used as the ICP etch mask.[45] Molds

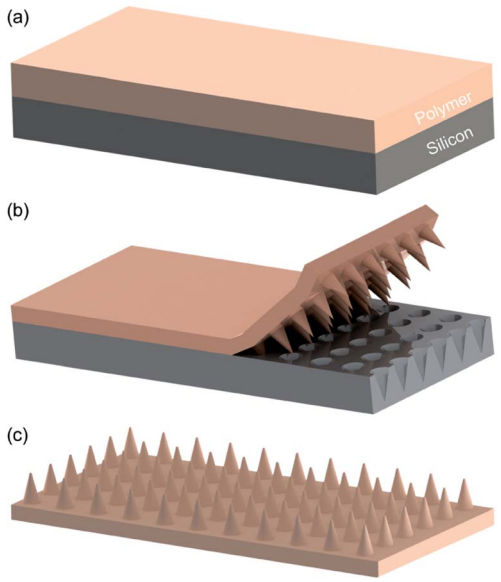

Fig. 2 Fabrication steps of the tapered polymer nanostructures. (a) PC solution is drop casted on the silicon mold, (b) the polymer film is then peeled from the silicon surface. (c) Nanostructured polymer film is obtained as a free-standing substrate. Drop casting is applied at ambient conditions which does not require a complex environment and allows the large-area production of nanostructured films.

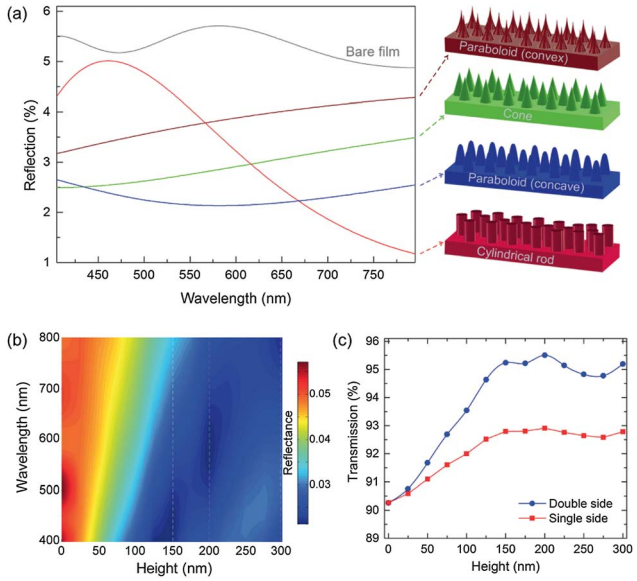

Fig. 3 Optical analysis of the tapered nanostructures. (a) Simulated reflection spectra for different shapes (cone, cylindrical rod, convex paraboloid, and concave paraboloid) for the 400–800 nm wavelength region. Structure period and height are kept constant and different shapes are compared with the bare film to find out the lowest average reflection. (b) The two-dimensional transmission map of tapered PC film (for 95 nm period) as a function of nanostructure height and wavelength of the incoming light. The vertical dashed lines correspond to the optimum heights of the nanostructures. (c) The calculated transmission values of single and double-side nanostructured PC films are given as a function of nanostructure height.

were used for several times after washing the remaining polymer. We imaged the PC nanostructures after using the mold ten times, and proved no deformations formed at the mold pores (Fig. S1†). This introduces a facile method of producing paraboloid PC nanostructures that offers a simple, low-cost, large-area, and reproducible fabrication of biomimetic surfaces.

PC nanostructures as antireflective and hydrophobic surfaces

To investigate the optimized fabrication parameters (*i.e.* shape and size) of the nanostructured PC antireflective surfaces, FDTD simulations were performed. Initially, simulations were derived to determine the best 3D shape for a fixed height (200 nm) and period (95 nm). Fig. 3a shows the simulation results of reflection by comparing a bare PC film with different surface architectures: cone, paraboloid (convex), cylinder, and paraboloid (concave). The average reflection observed for the bare polymer surface (no nanostructure) was about 5.5%. All the proposed nanostructures reduce the reflection compared to bare film. Paraboloids with a 95 nm period exhibit the lowest average reflection for PC material. Therefore, we chose and implemented paraboloids for antireflective surface design. In addition to the shape of the nanostructure, minimization of the reflection depends on the height and lattice constant. In our case, the lattice constant (~95 nm, which is appropriate for the wide range of spectrum) of the nanostructure array was dictated by the AAO membrane. To optimize the paraboloid (concave) height for the finest antireflection performance in the visible region, FDTD calculations were derived (Fig. 3b). The transmission increases starting from 150 nm up to 300 nm paraboloid heights. Maximum transmission points were predicted for three paraboloid heights; 150 nm, 200 nm, and 300 nm (Fig. 3c). We described the single-side fabrication of nanostructures, however the double-side nanostructured case, which could be important in unique applications, such as lens surfaces, can be obtained by further optimization of our technique. Therefore, we also provide simulation results for the double-side nanostructured case in Fig. 3c.

Based on the theoretical calculations, all experimental conditions were optimized to produce paraboloidal (concave) shaped polymer nanostructures. It is possible to tailor the heights of the structures by altering the etching duration during silicon mold production. Fig. 4a, c, and e present the SEM images of the fabricated PC paraboloid (concave) nanostructures which have average heights of about 150, 200, and 300 nm respectively, which correspond to the minimum reflection parameters confirmed by calculations (high resolution SEM images are also shown in Fig. 4b, d and f). The antireflection performance of the single-side nanostructured surfaces was compared with the bare film, as shown in Fig. 5a and b. We observed up to 4% difference for both the reflection and transmission values between the paraboloid structured films and bare films. Interestingly, the specular reflection and transmission of the surfaces with 150 nm and 300 nm structure heights are better than that with a height of 200 nm. This difference depends on the average homogeneity (uniformity) of the structures on the film. It also may arise due to the

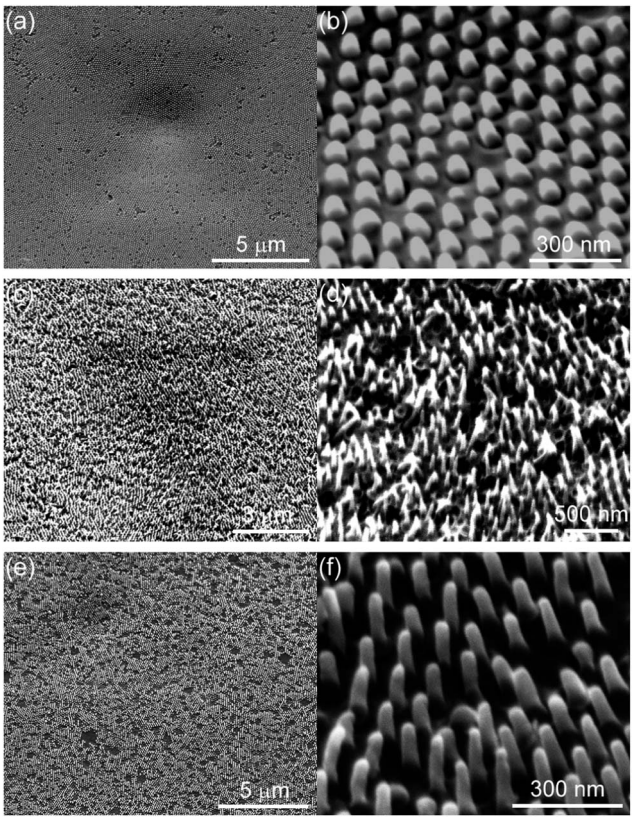

Fig. 4 SEM micrographs of the PC paraboloids for (a and b) 150 nm, (c and d) 200 nm, and (e and f) 300 nm heights. Images on the right column show high magnification images of the same nanostructures as in the left column. Imaging was performed at a 30° tilting angle to identify the tapered form of the nanostructures. The 150 nm nanostructured films appeared to be more uniform than the 200 nm and 300 nm nanostructured films. While extending the polymer nanostructures, bending may occur on the structures due to their soft nature.

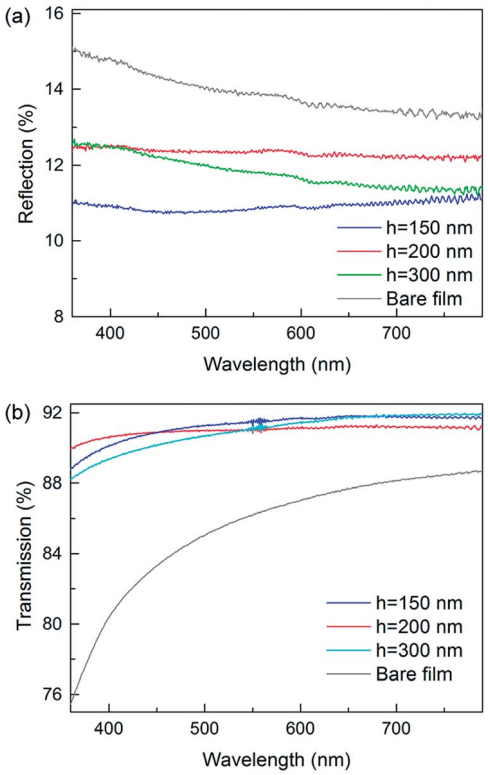

Fig. 5 Optical characterization of the nanostructured film. Measured (a) specular reflection and (b) transmission spectra for the 150 nm, 200 nm, 300 nm nanostructured films and bare film are given over a wavelength range of 350 nm to 800 nm. The 150 nm nanostructured film demonstrates the lowest reflection compared to the 200 nm and 300 nm nanostructured films. The optical transmission could reach 92% for the paraboloids with 150 nm height.

defects on the silicon surfaces which originate from the AAO mask. In addition, the measured and calculated transmission properties of the films are compared in Fig. S3,† consequently the FDTD simulations were confirmed by experimental findings. The designed nanostructures also display substantial increases in the transmission within the NIR region, which is critical for several applications, such as optical telecommunication in free space, and thermal imaging for security purposes (Fig. S2†).

Self-cleaning hydrophobic interfaces with high water contact angles, observed in various plants, insects, and animals, are among the most spectacular examples of natural functional surfaces.[46–48] The main reason of the improved hydrophobicity is the micro/nano-structure and the surface and low surface energy. The same phenomenon can be observed with the nanostructured PC films. In our studies bare PC films demonstrated a 120° water contact angle, whereas the nanostructured PC film exhibit increased hydrophobicity with a 145.4° water contact angle (CA) (Fig. S4a and b†). We observed that, besides the antireflection property, the nanostructured polymer films also display hydrophobic behavior, which could be important in self-cleaning surface applications and more reliable optical performances.

PC nanostructures as a surface-enhanced Raman scattering (SERS) sensing substrate

There has been a huge effort in the enhancing of Raman signals for very small amounts of biological and chemical compounds.[49,50] The detection of the analytes strongly depends on the interaction between the molecule and the Raman active area of the surface. However, it is still a big challenge to produce large area, sensitive, and reproducible SERS substrates. The order of enhancement factors varies between 10^5 and 10^8 for the reported SERS substrates, such as honeycomb structures, nanopillars, or nanotubes for *average SERS* experiments.[51–53]

Ordered hexagonal close-packed 3D nanoparaboloid surfaces are promising as large area, high resolution, and reproducible SERS substrates. A 150 nm nanostructured film as a SERS substrate and a bare polymer film as a control sample were coated with ~40 nm silver using thermal evaporation. A SEM image of the silver coated nanostructures is given in Fig. 6a. To reveal the Raman enhancement performance of the prepared paraboloid PC substrate, R6G was used. Raman signals are detected very sharply from the nanostructured surface, while the signals are hardly observed on the bare substrate (Fig. 6b). The main Raman active modes of the R6G were obtained.[54,55] The average enhancement factor was determined to be about 4.9×10^6 for the Raman peak at 613 cm^{-1} (experimental and calculation details are given in the ESI†).

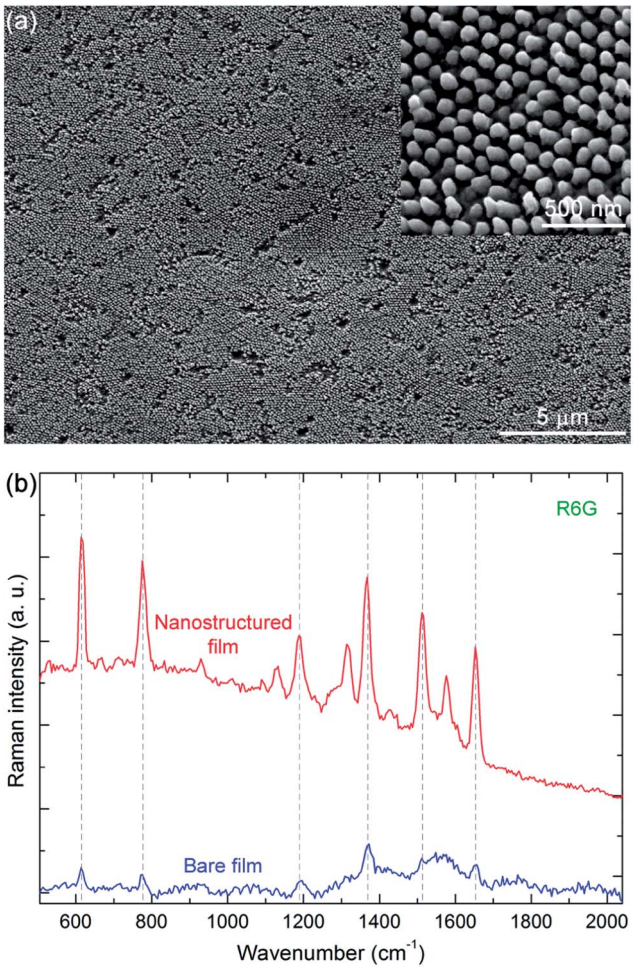

Fig. 6 Large-area nanostructured surfaces as a SERS substrate. (a) SEM image of the 40 nm silver coated nanostructured PC film. Inset shows a high magnification image of the same coated surface. 40 nm silver does not fill the lattice space between the nanostructures and the tapered form of the paraboloids are preserved. (b) SERS spectrum of the 10^{-7} M R6G generated by a silver coated 150 nm nanostructured film and the not enhanced Raman spectrum of the 2 mM R6G by the silver coated bare film are given. The Raman active modes of the R6G are significantly enhanced and highlighted by dashed lines, while the signals are barely detected on the bare film. In addition, the enhancement factor was calculated as 4.9×10^6 with respect to the peak at 613 cm^{-1}.

Conclusions and future directions

A facile, large-area and cost-effective method to produce nanostructured polymer surfaces was reported. The performance of the nanostructured polymer films was investigated on different surface applications. The fabricated nanoscale paraboloid structured polymer surfaces showed antireflectivity and nearly superhydrophobic properties. After coating with silver, the PC films also function as a sensitive SERS substrate. The experimental parameters were optimized in accordance with the FDTD simulations. Initially, the optimization of the nanostructure geometry was conducted *via* these simulations to yield the highest transmission. The optimum shape for improving the transmission of polymer films was determined to be paraboloid (concave) nanostructures. The nanostructure heights that provide the highest transmission were predicted as 150, 200, and 300 nm. Tapered features were formed on the silicon mold using an ICP etch process for desired pore sizes. The AAO membrane was used as an ICP etch mask, which provided a high density of hexagonally packed nanopores. The produced molds are suitable to use for multiple times (at least ten times). Polymer films were structured using these molds by drop casting. The fabricated paraboloid structures showed enhanced antireflective properties compared to bare polymer surfaces. The single-side nanostructured films showed up to 4% higher transmission than the bare films and the measured values are notably in agreement with the calculated ones. In addition, we observed that nanostructured PC films are highly hydrophobic with a water contact angle of 145.4°. Hexagonally packed paraboloid nanostructures also provided a large Raman active area that rendered them useful as SERS substrates with an average enhancement factor of 4.9×10^6. The demonstrated fabrication method of nanostructured polymer films may be used in sensing, optic and optoelectronic applications.

Acknowledgements

We thank to Adem Yildirim and Fahri Emre Ozturk for fruitful discussions. We also thank to Sevde Altuntas for the preparation of AAO membranes. This work was supported by the TUBITAK Grant no. 110M412 and 111T696. M.B. acknowledges partial support from the Turkish Academy of Sciences (TUBA).

Notes and references

1 Y. Li, J. Zhang and B. Yang, *Nano Today*, 2010, **5**, 117–127.
2 L. Feng, S. Li, Y. Li, H. Li, L. Zhang, J. Zhai, Y. Song, B. Liu, L. Jiang and D. Zhu, *Adv. Mater.*, 2002, **14**(24), 1857–1860.
3 X. Yao, Y. Song and L. Jiang, *Adv. Mater.*, 2011, **23**, 719–734.
4 C. M. Chen, C. L. Chiang, C. L. Lai, T. Xie and S. Yang, *Adv. Funct. Mater.*, 2013, **23**, 3813–3823.
5 W. K. Cho and I. S. Choi, *Adv. Funct. Mater.*, 2008, **18**, 1089–1096.
6 Y. H. Ko and J. S. Yu, *Opt. Express*, 2011, **19**(1), 297–305.
7 H. Xu, N. Lu, D. Qi, J. Hao, L. Gao, B. Zhang and L. Chi, *Small*, 2008, **4**(11), 1972–1975.
8 H. Deniz, T. Khudiyev, F. Buyukserin and M. Bayindir, *Appl. Phys. Lett.*, 2011, **99**, 183107.
9 Y. Li, J. Zhang, S. Zhu, H. Dong, F. Jia, Z. Wang, Z. Sun, L. Zhang, Y. Li, H. Li, W. Xu and B. Yang, *Adv. Mater.*, 2009, **21**, 4731–4734.
10 P. Aurang, O. Demircioglu, F. Es, R. Turan and H. E. Unalan, *J. Am. Ceram. Soc.*, 2013, **96**(4), 1253–1257.
11 Y. Liu, T. Lai, H. Li, Y. Wang, Z. Mei, H. Liang, Z. Li, F. Zhang, W. Wang, A. Y. Kuznetsov and X. Du, *Small*, 2012, **8**(9), 1392–1397.
12 W. Joo, H. J. Kim and J. K. Kim, *Langmuir*, 2010, **26**(7), 5110–5114.
13 H. Budunoglu, A. Yildirim and M. Bayindir, *J. Mater. Chem.*, 2012, **22**, 9671–9677.
14 A. Yildirim, T. Khudiyev, B. Daglar, H. Budunoglu, A. K. Okyay and M. Bayindir, *ACS Appl. Mater. Interfaces*, 2013, **5**, 853–860.

15 X. Li, J. Gao, L. Xue and Y. Han, *Adv. Funct. Mater.*, 2010, **20**, 259–265.
16 Y. J. Lee, D. S. Ruby, D. W. Peters, B. B. McKenzie and J. W. P. Hsu, *Nano Lett.*, 2008, **8**(5), 1501–1505.
17 F. Jiao, Q. Huang, W. Ren, W. Zhou, F. Qi, Y. Zheng and J. Xie, *Microelectron. Eng.*, 2013, **103**, 126–130.
18 T. Kraus, D. Brodoceanu, N. P. Perez and A. Fery, *Adv. Funct. Mater.*, 2013, **23**, 4529–4541.
19 U. Schulz, P. Munzert, F. Rickelt and N. Kaiser, *Thin Solid Films*, 2013, **532**, 119–122.
20 W. R. Childs, M. J. Motala, K. J. Lee and R. G. Nuzzo, *Langmuir*, 2005, **21**, 10096–10105.
21 S. S. Oh, C. G. Choi and Y. S. Kim, *Microelectron. Eng.*, 2010, **87**, 2328–2331.
22 Y. M. Song, S. J. Jang, J. S. Yu and Y. T. Lee, *Small*, 2010, **6**(9), 984–987.
23 I. Yamada, N. Yamashita, K. Tani, T. Einishi, M. Saito, K. Fukumi and J. Nishii, *Appl. Phys. Express*, 2012, **5**, 082502.
24 I. Wathuthanthri, Y. Liu, K. Du, W. Xu and C. H. Choi, *Adv. Funct. Mater.*, 2013, **23**, 608–618.
25 R. D. Mundo, M. Troia, F. Palumbo, M. Trotta and R. d'Agostino, *Plasma Processes Polym.*, 2012, **9**, 947–954.
26 S. Ji, J. Park and H. Lim, *Nanoscale*, 2012, **4**, 4603–4610.
27 C. C. Hong, S. Y. Huang, J. Shieh and S. H. Chen, *Macromolecules*, 2012, **45**, 1580–1586.
28 J. Shklovsky, L. Engel, Y. Sverdlov, Y. Shacham-Diamand and S. Krylov, *Microelectron. Eng.*, 2012, **100**, 41–46.
29 A. Kaless, U. Schulz, P. Munzert and N. Kaiser, *Surf. Coat. Technol.*, 2005, **200**, 58–61.
30 G. Ehret, E. Buhr, S. Gabler and H. M. Bitzer, *Plasma Processes Polym.*, 2009, **6**, S840–847.
31 R. Kasztelanic, I. Kujawa, R. Stepien, K. Harasny, D. Pysz and R. Buczynski, *Infrared Phys. Technol.*, 2013, **60**, 1–6.
32 J. Martin, C. Mijangos, A. Sanz, T. A. Ezquerra and A. Nogales, *Macromolecules*, 2009, **42**, 5395–5401.
33 T. Nakanishi, T. Hiraoka, A. Fujimoto, T. Okino, S. Sugimura, T. Shimada and K. Asakawa, *Jpn. J. Appl. Phys.*, 2010, **49**, 075001.
34 H. Park, D. Shin, G. Kang, S. Baek, K. Kim and W. J. Padilla, *Adv. Mater.*, 2011, **23**, 5796–5800.
35 C. J. Ting, M. C. Huang, H. Y. Tsai, C. P. Chou and C. C. Fu, *Nanotechnology*, 2008, **19**, 205301.
36 F. Buyukserin, M. Aryal, J. Gao and W. Hu, *Small*, 2009, **5**(14), 1632–1636.
37 J. T. Kwon, H. G. Shin, Y. H. Seo, B. H. Kim, H. G. Lee and J. S. Lee, *Curr. Appl. Phys.*, 2009, **9**, e81–85.
38 L. F. Boesel, C. Greiner, E. Arzt and A. del Campo, *Adv. Mater.*, 2010, **22**, 2125–2137.
39 D. Rajput, L. Costa, K. Lansford, A. Terekhov and W. Hofmeister, *ACS Appl. Mater. Interfaces*, 2013, **5**, 1–5.
40 A. M. Bowen, M. J. Motala, J. M. Lucas, S. Gupta, A. J. Baca, A. Mihi, A. P. Alivisatos, P. V. Braun and R. G. Nuzzo, *Adv. Funct. Mater.*, 2012, **22**, 2927–2938.
41 K. Choi, S. H. Park, Y. M. Song, Y. T. Lee, C. K. Hwangbo, H. Yang and H. S. Lee, *Adv. Mater.*, 2010, **22**, 3713–3718.
42 W. Y. Chang, K. H. Lin, J. T. Wu, S. Y. Yang, K. L. Lee and P. K. Wei, *J. Micromech. Microeng.*, 2011, **21**, 035023.
43 C. C. Yu, Y. T. Chen, D. H. Wan, H. L. Chen, S. L. Ku and Y. F. Chou, *J. Electrochem. Soc.*, 2011, **158**(6), J195–J199.
44 R. C. Furneaux, W. R. Rigby and A. P. Davidson, *Nature*, 1989, **337**, 147.
45 Z. Huang, G. Meng, Q. Huang, B. Chen, C. Zhua and Z. Zhanga, *J. Raman Spectrosc.*, 2013, **44**, 240–246.
46 X. Yao, L. Xu and L. Jiang, *Adv. Funct. Mater.*, 2010, **20**, 3343–3349.
47 Y. L. Zhang, H. Xia, E. Kim and H. B. Sun, *Soft Matter*, 2012, **8**, 11217–11231.
48 T. Darmanin, E. T. de Givenchy, S. Amigoni and F. Guittard, *Adv. Mater.*, 2013, **25**, 1378–1394.
49 S. Ayas, H. Guner, B. Turker, O. O. Ekiz, F. Dirisaglik, A. K. Okyay and A. Dana, *ACS Nano*, 2012, **6**(8), 6852–6861.
50 J. P. Singh, H. Y. Chu, J. Abell, R. A. Trippa and Y. Zhao, *Nanoscale*, 2012, **4**, 3410–3414.
51 W. Leng and P. J. Vikesland, *Anal. Chem.*, 2013, **85**, 1342–1349.
52 J. D. Caldwell, O. Glembocki, F. J. Bezares, N. D. Bassim, R. W. Rendell, M. Feygelson, M. Ukaegbu, R. Kasica, L. Shirey and C. Hosten, *ACS Nano*, 2011, **5**(5), 4046–4055.
53 D. C. Rodrigues, G. F. S. Andradeb and M. L. A. Temperini, *Phys. Chem. Chem. Phys.*, 2013, **15**, 1169.
54 E. C. Le Ru, E. Blackie, M. Meyer and P. G. Etchegoin, *J. Phys. Chem. C*, 2007, **111**, 13794–13803.
55 Y. Yang, Z. Y. Li, K. Yamaguchi, M. Tanemura, Z. Huang, D. Jiang, Y. Chen, F. Zhoub and M. Nogami, *Nanoscale*, 2012, **4**, 2663–2669.

